Heliyon 5 (2019) e02323

Contents lists available at ScienceDirect

Heliyon

journal homepage: www.heliyon.com

Functionalized locust bean pod (*Parkia biglobosa*) activated carbon for Rhodamine B dye removal

Olugbenga Solomon Bello [a,b,*], Kayode Adesina Adegoke [c,**], Oluwafunmilayo Oluwapamilerin Sarumi [a], Olasunkanmi Seun Lameed [a]

[a] Department of Pure and Applied Chemistry, Ladoke Akintola University of Technology, P.M.B. 4000, Ogbomoso, Oyo State, Nigeria
[b] Department of Physical Sciences, Industrial Chemistry Programme, Landmark University, Omu-Aran, Nigeria
[c] Department of Chemistry, University of Pretoria, Pretoria, 0002, South Africa

ARTICLE INFO

Keywords:
Environmental science
Locust bean pod
Rhodamine B dye
Adsorption
Kinetics
Isotherms
Thermodynamics

ABSTRACT

Activated carbon prepared from *locust bean* husk was modified using ortho-phosphoric acid (ALBP) and used to scavenge Rhodamine B (RhB) dye from aqueous solutions. Characteristic features of the adsorbents were investigated using SEM, FTIR, pH_{pzc} and Boehm Titration (BT) techniques respectively. Batch studies were used to determine the influences of contact time, temperature and initial Rh–B dye concentrations. Adsorption data were analysed using four different isotherm models. The maximum monolayer adsorption capacity of 1111.1 mgg^{-1} was obtained for RhB dye adsorption. The kinetics of the adsorption process was studied using pseudo-first-order, pseudo-second-order Elovich and intraparticle diffusion models respectively. The experimental data was best described by pseudo-second-order kinetic model. Favourability of the process of adsorption was also established by the separator factor (R_L) value ranging from 0 and 1, while the mean energy of adsorption (E_a) was 1.12 $kJmol^{-1}$ suggesting that the removal of Rh–B dye from aqueous solution followed a physisorption process. For the thermodynamic investigations, the positive values of ΔS (280.956 $Jmol^{-1}K^{-1}$) indicates the affinity of adsorbent for the Rh–B dye uptake and increase randomness at the solid–solution interface during adsorption of Rh–B dye onto the surface of the active sites of ALBP. The negative value of ΔG (-31.892 to -26.355 $kJmol^{-1}$) depicts the spontaneity and feasibility of the adsorption process. The cost analysis provides a simple proof that ALBP (42.52 USD per kg) is approximately six times cheaper than Commercial Activated Carbon, CAC (259.5 USD per kg). The present study therefore established the suitability of ALBP for effective removal of Rh–B dye from aqueous solutions.

1. Introduction

Effluents discharged from industries like cosmetics, pulp mills, paper, rubber, paints, printing, textiles, pharmaceuticals, plastics, foods and leather have recently become a global problem. These industries indiscriminately use large volume of dyes and generate abundant wastewater which contaminates the environment. Their presence has been rated as the most notorious and severe pollutants amongst all other sectors owing to the fact that textile industries are the major dye consumers in every of their products [1, 2]. Among the various organic compounds released into water bodies, pigments and dyes are largely abundant consisting hazardous water pollutant that has progressively threatened global peace. Dyes are venomous and non-biodegradable, their presence in the water even at very minute concentration pose mutagenic, teratogenic and carcinogenic effects on both aquatic life, humans, and the ecosystem as a whole [3, 4, 5, 6]. Conventional treatment technologies (adsorption, biological treatment, chemical oxidation, coagulation, and reverse osmosis) for dye adsorption have been investigated extensively [2, 3, 4, 5, 6]. Adsorption technology remains sustainable, efficient, and the safest technique for combating challenges emanating from alarming increase in urbanization and industrialization.

Activated carbon (AC) is known for its superior surface areas and microporous structures, which contribute to their higher adsorption capacities. Thus, its wider applications as adsorbent can be attributed to such properties. Despite such robust attributes, it suffers major challenge that has to do with capital cost. This serves as major drawbacks to its

* Corresponding author.
** Corresponding author.
E-mail addresses: osbello06@gmail.com (O.S. Bello), kwharyourday@gmail.com (K.A. Adegoke).

https://doi.org/10.1016/j.heliyon.2019.e02323
Received 6 December 2018; Received in revised form 25 July 2019; Accepted 13 August 2019

usage in the last decades. This important problem has given birth into all-time increasing researches into finding feasible, cheaper, affordable and more readily available adsorbents [2, 5, 7, 8, 9]. On this note, non-conventional adsorbents have been fabricated over the years for removal of both synthetic and natural dyes [2, 3, 4, 5, 6, 10, 11, 12, 13, 14].

However, *Parkia biglobosa*, also known as the African locust bean is a dicotyledonous angiosperm belonging to the family *Fabaceae*. It is categorized under spermatophytes i.e vascular plants [15, 16, 17, 18]. The pods of the tree, commonly referred to as locust beans, are pink in the beginning and turn dark brown when fully mature. They are 30–40 centimetres long on average, with some reaching lengths of about 45 centimetres. Each pod can contain up to 30 valuable seeds [15, 16, 17, 18], and once these seeds are harvested, the pods are thrown away as garbage which accumulates within the shorted possible time and become a nuisance in the environment. Whenever they are burnt, they smell horribly, thus causing pollutions. At the fall of the rain, their decays gave irritating odours which are unbearable to the ecosystem. This implies that these pods are disposed as zero value wastes in West African countries and its management in the environment is a concern in both rainy and dry seasons. Therefore, the application of these locus beans wastes as potential carbon sources for producing AC is at present a fascinating topic owing to its availability at zero/no cost. Additional important advantages are eradication of its accumulation, decaying or burning, thereby cleaning the environment in managing agricultural wastes. One of the methods employed in improving the adsorption capacity of this waste is through chemical activation using acids. This was employed in this study. In this process, hydrogen ions are replaced with changeable ions. The formation of these changeable ions create a porous structure and high surface area, which eventually increase its adsorption capacity [19, 20, 21, 22, 23, 24].

Rhodamine B (Rh–B) dye is a basic dye, extensively employed in printing, painting, leather and textile industries [25, 26, 27, 28]. It is an amphoteric dye, listed in the class of the xanthene dye causing harmful effects such as acute oral toxicity. When swallowed, it causes damage to the eyes or skin irritation and hazardous to the aquatic organism with long-term effects. Therefore, the treatment of effluent containing Rh–B dye becomes paramount before discharging them into water streams so as to protect the aquatic organism and make the environment safer for the populace [29]. According to the EPA [30], Rhodamine B dye is a list I inert ingredient. The criteria used to place chemicals on list I are: carcinogenicity, adverse reproductive effects, neurotoxicity or other chronic effects, and developmental toxicity [30, 31]. Moreso, its usage in seed treatment should not exceed 2 % by weight of the formulated product and 60 ppm on the treated seed [30]. Also, its use in the environment requires tracer concentrations not exceeding 1–2 mg L^{-1} persisting for a period in excess of 24 h in the groundwater at the point of groundwater withdrawal or discharge [32]. Rh–B dye is known to be highly toxic to fish with LC_{50} of 83.9 mg L^{-1} studied for *Cyprinodon variegatus* [27, 33]. Animal testing on rats reported tumours growth on the site of application, and also resulted in reproductive toxicity such as stunted foetuses [33]. However, many adsorbents have been used for scavenging Rh–B dye with adsorption capacity ranges from 3.04 mg/g to 666.67 mg/g [13, 27, 29, 34, 35, 36, 37, 38, 39, 40, 41, 42], but the ability of locus been pod has not been reported previously, thus making the utilization of activated carbon prepared from locus bean pod a novel adsorbent for Rh–B dye removal.

This study is therefore aimed at converting locus bean pod biomass wastes into AC by preparing a superior functionalized (acid modified) adsorbent with high porosity and surface area for Rh–B dye sequestration from the aqueous solutions. To the best of our knowledge, there are no documented reports on the utilization of functionalized locus bean pod for Rh–B dye adsorption from the aqueous solutions, thus establishing the novelty of this study focusing on the potential use of locus bean pod as adsorbent for Rh–B dye removal. The study of different operational variables, including contact time, initial Rh–B dye concentration, and pH were carefully investigated. Kinetic, isotherm and thermodynamic parameters controlling the process of adsorption were also investigated.

2. Materials and methods

2.1. Chemicals

The chemicals employed for this investigation are: orthophosphoric acid (H_3PO_4), Rhodamine B dye, NaOH, $NaHCO_3$, Na_2CO_3 and HCl. The chemicals were of analytical grade and were therefore used without further purification.

2.2. Adsorbate solution preparation

To prepare 1000 mg/L of Rh–B dye stock solution, accurately weighed 1.0 g powdered Rh–B dye was dissolved in 1000 ml of distilled water. Other five concentrations (200–1000 mg/L) were prepared from the stock by serial dilution. These solutions were used for subsequent experiments. The properties of Rh–B dye are listed in Table 1.

2.3. Locust bean pod preparation

Locust bean pods were collected from agricultural farm within Ogbomoso metropolis, Nigeria; they were first washed thoroughly with tap water. Thereafter the pods were further washed with distilled water to get rid of suspended impurities and then dried in an oven to constant weight. The pod samples were grounded, sieved into various mesh sizes and kept in an airtight container for future use and labelled as RLBP.

2.4. Preparation of functionalized activated carbon

A carefully weighed 25.0 g RLBP was impregnated in a beaker containing 500 cm^3 of 0.3 mol/dm^3ortho-phosphoric acid (H_3PO_4). Functionalization procedure was based on the previous procedure [4, 43]. The mixture was thoroughly stirred and heated on a hot plate until uniform slurry was obtained. This was then transferred into an evaporating dish and heated to 300 °C in a muffle furnace for 30 minutes. This was allowed to cool prior to washing with distilled water for maintaining a pH of 6.8. Following this process is drying in an oven at 105 °C for 6 hrs in order to obtain a constant weight. The resulting products were then grounded into fine powder and thereafter sieved using 106 μm mesh size to obtain a very fine powdered acid activated locust bean husk pod (ALBP). This was finally kept in air-tight containers for subsequent use and labelled as ALBP. Ortho-phosphoric acid (PA), promotes bond cleavage in agricultural waste biomass through dehydration at low temperature followed by extensive cross linking that binds volatile matter into the carbon products and thus increases the carbon yield. The mechanism of PA activation of biomass occurs through various steps: cellulose de-polymerization, biopolymer dehydration, formation of aromatic rings and elimination of phosphate groups. This produces activated carbon with good yields and high surface areas. Activation condition thus depends on the nature of the precursor, i.e on the relative amounts of cellulose, hemicelluloses, lignin and ashes [4, 41, 43].

Table 1
List of properties of Rh–B dye (Adsorbate).

IUPAC name	[9-(2-carboxyphenyl)-6-diethylamino-3-xanthenylidenediethylammonium chloride]
Common name	Rhodamine B
CI name	Basic violet 10
CI number	45170
Max wavelength	543 nm
Molecular formula	$C_{28}H_{31}ClN_2O_3$
Molecular weight	479.02 $gmol^{-1}$

2.5. Characterization

2.5.1. Characterization of RLBP and ALBP

2.5.1.1. Fourier transform infrared spectroscopy. The spectra of raw and acid activated locus bean husks were recorded on a PerkinElmer FTIR-2000 Fourier transform infrared (FTIR) spectrometer (Shimadzu Model IRPrestige-21 Spectrophotometer). The spectra measurement was taken within the range of 4000 to 400 cm^{-1} using KBr disc. The spectroscopic analysis was employed to investigate the surface chemistry of RLBP and ALBP powders. The FTIR spectra gave detail characteristics' functional group (s) on the surfaces of both RLBP and ALBP.

2.5.1.2. Scanning electron microscopy (SEM). The surface morphology of the samples was examined using scanning electron microscope (SEM; Model VPFESEM Supra 35VP). SEM is a brand of electronic microscope which apply rays of focused low energy electron to generate magnified images of a sample [43]. Interactions of the shaft of electron with the atomic constituents of the sample results in generation of various signals. Information regarding the sample's surface property, constituents and its scenery are inferred from the signals generated by SEM.

2.5.1.3. Determination of point of zero charge (pH_{pzc}). For the determination of pH_{pzc} of the adsorbent, 0.05 g of ALBP was added to the 200 ml solution of 0.1M NaCl of a known initial pH; the pH was adjusted with NaOH or HCl. The sample holder was corked and placed in a shaker, made to be agitated at 250 rpm for 24 h. The final pH was then measured. In order to determine the pH_{pzc}, a graph of pH difference, ΔpH (final pH − initial pH) was plotted against the initial pH. The pH_{pzc} exists when pH does not change upon contact with the adsorbent(s) [9, 27, 36, 41].

2.5.1.4. Determination of oxygen containing functional groups (Boehm titration). This study used Boehm titration method to determine the oxygen containing functional groups [44, 45]. Four portions of 1.0 g each of RLBP and ALBP samples were kept in contact with separate solution of 10–15 ml of 0.1 M NaOH, 0.1 M $NaHCO_3$ and 0.05 M Na_2CO_3 for an acidic groups and 0.1 M HCl for a basic groups composites respectively at ordinary temperature for 48 h as earlier reported by Ekpete and Horsfall [45]. Afterwards, the resulting aqueous solutions were back-titrated with 0.1 M HCl for acidic and 0.1 M NaOH for basic groups. The types and numbers of acidic sites were calculated using previous procedure [9, 41]. Briefly, for the determination of the numbers and types of acidic sites, certain considerations were made. NaOH neutralizes carboxylic, lactone and phenolic groups, Na_2CO_3 neutralizes carboxylic and lactonic groups and that $NaHCO_3$ neutralizes only carboxylic groups. The amount of oxygen-containing-functional groups, F_x, is calculated using the following equations:

$$F_x = \frac{(V_{bx} - V_{ex})}{m_x} \times M_t \times D_F \quad (1)$$

$$D_F = \frac{initial\ volume}{selected\ volume\ for\ titration} \quad (2)$$

Where F_x (m $molg^{-1}$) is the amount of oxygen containing functional groups, V_{bx} is the volume of titrant used to titrate the blank, V_{ex} is the volume of the titrant used to titrate the extract, M_t is the molarity of the titrant used, D_F is the dilution factor [9, 41].

2.5.1.5. Batch adsorption experiment. The removal of Rh–B dye was studied at various temperatures (303 K, 313 K and 323 K) using the batch technique to investigate the effects of operational parameters such as initial dye concentration, contact time, adsorbent dose, and solution temperatures. The adsorbent dosage used throughout the adsorption process was 0.1 g of ALBP and this was observed at four initial dye concentrations: 200, 400, 600, 800 and 1000 mg/L respectively. Five (5) sets of 100 ml Erlenmeyer flasks containing the mixture of 0.1 g of ALBP and the Rh–B dye solution of different initial dye concentrations were carefully arranged in the shaker and then agitated at 120 rpm. Each of the flasks was continuously agitated in a water bath shaker for 2 h at each temperature until the equilibrium was attained. This was done by filling the bath shaker with enough water to the level of the pre-arranged flasks' solutions so as to make the solution temperature uniform to that of the shaker at a specified working temperature; until equilibrium was reached. Small quantity of sample solutions was collected using a 10 ml syringe at pre-determined interval of time after agitations to determine the percentage removal of Rh–B dye from the solution. The residual concentrations of the dye solutions were calculated by measuring the absorbance at a wavelength of 554 nm using the UV/vis spectrophotometer (Model 6715: Jenway). The amount of Rh–B dye uptake and Rh–B dye percentage removal at equilibrium were calculated using Eqs. (3) and (4) respectively:

$$q_e = \frac{(Co - Ce)V}{m} \quad (3)$$

$$\%\ removal = \left[\frac{(Co - Ce)}{Co}\right] \times 100\% \quad (4)$$

Where "q_e is the amount of dye adsorbed by the activated carbon, C_o is the initial equilibrium concentration of adsorbate (mg/L), and C_e is the equilibrium concentration of dye solution (mg/L), W is the weight of the adsorbent (g), and V is the initial volume of dye solution used (dm^3)" [5].

2.5.1.6. Effect of agitation time, initial Rh–B dye concentration and solution temperature. In order to study the effects of agitation time and initial Rh–B dye concentration adsorbed, 100 mL of Rh–B dye solutions with initial concentrations of 200–1000 mg/L were prepared and arranged in sequence of 200-mL Erlenmeyer flasks. An equal mass of 0.10 g of ALBP was added to each flask. These flasks were covered with glass stoppers and placed in an isothermal waterbath shaker at 303 K and rotation speeds of 120 rpm were maintained throughout until equilibrium was attained. The effects of solution temperature on the process of Rh–B dye adsorptions were investigated by changing the water bath temperature controller to 303, 313 and 323 K respectively.

2.5.1.7. Adsorption isotherm and kinetics. The interaction between the adsorbate (Rh–B dye) and the adsorbent (ALBP) were analyzed via four isotherm models: Langmuir [46], Freundlich [47], Dubinin-Radushkevich (D-R) [5, 48, 49] and Temkin [50] models. Adsorption kinetic study offers useful information on the pathways and reaction mechanisms of the reaction as it relates the rate of the adsorption with the adsorbate concentration in the solution. Kinetics of adsorption of Rh–B dye onto ALBP were tested using pseudo-first order (PFO) [51], pseudo-second order (PSO) [52], Elovich [53, 54] and intraparticle diffusion (IPD) [55] models. Isotherm and kinetic parameters for Rh–B dye adsorption on ALBP are listed in Table 2.

2.5.1.8. Test of kinetic models. The model fitness or applicability was tested by using the Sum of Error Squares (SSE, %) in addition to the correlation regression (R^2) values that are common to all kinetic models, Adsorption of Rh–B dye molecule onto ALBP was determined at various initial dye concentrations. However, all kinetic models employed for the kinetic studies of the adsorption processes were verified by SSE (%) calculated using Eq. (16):

$$SSE\ (\%) = \sqrt{\sum \frac{\left(q_{e,exp} - q_{e,calc}\right)^2}{N}} \quad (16)$$

Where N is the number of data points. The goodness of the fit depends on the value of R^2 and SSE value, the lower the value of SSE, the higher the

Table 2
Adsoption isotherm and kinetic models.

Adsorption model	Type	Expression	Refs.
Isotherm	Langmuir	$\frac{C_e}{q_e}=\frac{1}{q_m C_e}+\frac{1}{K_L q_m}$ (5) $R_L=\left[\frac{1}{(1+K_L Co)}\right]$ (6)	[46]
	Freundlich	$\ln q_e=\frac{1}{n}\ln C_e+\ln K_f$ (7)	[47]
	Temkin	$q_e = B\ln K_T + B\ln C_e$ (8)	[48]
	Dubinin–Radushkevich isotherm	$\ln q_e=\ln q_m+\beta\varepsilon^2$ (9) $\varepsilon = RT\left[1+\frac{1}{C_e}\right]$ (10) $E=\frac{1}{\sqrt{2\beta}}$ (11)	[50] [5, 49]
Kinetics	Pseudo-first-order	$\ln(q_e-q_t)=\ln q_e - K_1$ (12)	[51]
	Pseudo-second order	$\frac{t}{q_e}=\frac{1}{K_2 q_e}+\frac{1}{q_e}t$ (13)	[52]
	Elovich	$q_t=\frac{1}{\beta}\ln(\alpha\beta)+\frac{1}{\beta}\ln t$ (14)	[53, 54]
	Intra-particle diffusion	$q_t + K_{diff}t^{1/2}+C$ (15)	[41, 55]

Where "C_e is the adsorbate concentration at equilibrium (mg/L),q_e is the amount of adsorbate adsorbed per unit mass of adsorbent ($mg.g^{-1}$), q_m is the maximum monolayer adsorption capacity of the adsorbent ($mg.g^{-1}$), K_L; the Langmuir adsorption constant ($L.mg^{-1}$). C_o is the highest initial solute concentration; whereas, R_L value implies the adsorption is unfavorable {(R_L>1), linear ($R_L = 1$), favorable (0 <R_L< 1), or irreversible ($R_L = 0$)}. K_f is the Freundlich isotherm constant (($mg.g^{-1}$) ($L.mg^{-1}$); n, the heterogeneity factor. The slope of 1/n ranging between 0 and 1 is a measure of adsorption intensity, which becomes more heterogeneous as the values get closer to zero. B = R_T/b is the constant related to the heat of adsorption ($L.mg^{-1}$); T is absolute temperature; R is universal gas constant (8.314 J/mol K); K_T, equilibrium binding constant ($L.mg^{-1}$). β a constant related to the adsorption energy (mol^2/kJ^2); ε is the Polanyi potential, E is adsorption energy (when value of E is between 1 and 8 kJ/mol, it implies a physical adsorption while value between 9 and 16 kJ/mol means a chemical adsorption [49]. Whereas, $q_t$is the amount of solute adsorb per unit weight of adsorbent at time t (mgg^{-1}), K_1 and K_2 are the pseudo-first order and pseudo-second order kinetics rate constants (min^{-1}). Whereas, α is the initial desorption rate [mg (g min)$^{-1}$], β, the desorption constant ($g.mg^{-1}$). The 1/b value denotes the number of available sites for adsorption and the value of (1/β); (ln αβ) shows quantity of adsorption when (ln t) equal to zero. C is the intercept and reflects the boundary layer effect of the plot q_t against $t^{1/2}$. K_t(mg/g $h^{1/2}$) denotes the intra-particle diffusion rate constant; $t^{1/2}$, the half-adsorption time ($h^{1/2}$). For intra-particle diffusion to be the only rate determining step, then the regression of q_t against $t^{1/2}$ must be linear and should pass through the origin, otherwise, it then implies that the intra-particle diffusion is not the only rate-controlling step" [5].

value of R^2; the better the goodness of the fit [56].

2.5.1.9. Adsorption thermodynamic studies. The changes in energy that occurred during the process of adsorption were determined using thermodynamic parameters. In this study, changes in entropy (ΔS^o), enthalpy (ΔH^o), and Gibb free energy (ΔG^o) were used for investigating the process adsorption using relations in Eq. (17).

$$\ln K_L = \frac{\Delta S^o}{R} - \frac{\Delta H^o}{RT} \quad (17)$$

Where: "K_L is the Langmuir adsorption constant (L/mg), ΔS^o is the change in standard entropy (kJ/mol K), R is the Universal gas constant (8.314 J/mol K), ΔH^o is the change in standard enthalpy (kJ/mol K) whereas T is the absolute solution temperature (K)". Hence, ΔS^o and ΔH^o were determined from the intercept and slope of *In K_L* plotted against *1/T*. It should be recalled that when the value of ΔH^o is positive, it implies that the process of adsorption is endothermic whereas a negative value of ΔH^o means an exothermic reaction. Similarly, if ΔS^o value is positive it indicates an increased randomness at the solid-solution interfaces occurring during the process of adsorption in addition to the adsorbent's affinity towards RhB dye [57, 58, 59]. Also, the spontaneous nature in the process of adsorption suggests that the value of ΔG^o is negative at the temperature under study and vice-versa. ΔG^o was evaluated using Eq. (18):

$$\Delta G^o = -RT\ln K_L \quad (18)$$

The magnitude of activation energy, E_a, determined the adsorption nature and the Arrhenius equation (Eq. 19) remains an important phenomenon to ascertain if the process of adsorption is physically or chemically controlled. For a physically controlled process (i.e physisorption), E_a ranges from 5 to 40 kJ/mol while for the chemically controlled process the E_a must be higher than 40 kJ/mol and exist within 40–800 kJ/mol [60].

$$\ln K_2 = \ln A - \frac{E_a}{RT} \quad (19)$$

Where: K_2 is the rate constant obtained from the pseudo-second order kinetic model (g/mg min). A is the Arrhenius factor, E_a is the Arrhenius activation energy of adsorption (kJ/mol). Thus, ln K_2 versus 1/T plot should give a linear graph having $-E_a/R$ as the slope of the graph.

3. Results and discussions

3.1. Characterization of RLBP and ALBP adsorbents

3.1.1. Surface chemistry of RLBP and ALBP adsorbents

Fig. 1 shows the FTIR spectra of Locust bean pod before (Fig. 1a) and after activation (Fig. 1b). Observations from Fig. 1 showed a shift, broadening and disappearance of the peaks after activation of the adsorbent. The disappearance of some functional groups in the adsorbent reveals that the functional groups are unstable due to increase in temperature during the activation process [61, 62]. Table 3 shows the comparative features of absorption bands for each FTIR spectra of RLBP and ALBP with their differences and various assignments. The long bandwidths between 3800 and 3755 cm^{-1} was assigned to asymmetric stretching of O–H while the peak between 3431 and 3404 cm^{-1} were attributed to the bonded O–*H group*. The aliphatic C–*H group* was observed at 2934 –2922 cm^{-1} while aliphatic C=C was detected at 1618 –1601 cm^{-1} respectively. Other peaks observed are 2376 cm^{-1} for –C=N stretching, 1705 –1699 cm^{-1} assigned to -C-O stretching of ketone, 1460 –1452 cm^{-1} attributed to C=C stretching in the aromatic ring, C–H bonding in alkane was observed at 1369 cm^{-1} and SO_3 stretching were detected at bandwidths of 1231 –1229 cm^{-1}. The reduction in the peaks in bonded O–H and aromatic groups were as a result of oxidative degradations occurring during chemical impregnations and heating stages [9, 63].

3.1.2. Surface morphology of RLBP and ALBP adsorbents

The SEM images reveal the surface texture of locust bean pod before and after acid activation as shown in Fig. 2 (a, b). From Fig. 2a, it is obvious that RLBP surface was rough and the presence of pores were not evident, while ALBP (Fig. 2b) has well-developed visible pores due to the H_3PO_4 modification. The effects of activating agent at high temperature broke down the lignocellulosic materials followed by volatilization of the volatile compound (s) [9, 63]. There is increase in the rate of reaction during the C–H_3PO_4 activation processes, which resulted into carbon "burn off," leaving behind a formation of the good porous surface on the ALBP sample. C–H_3PO_4 reaction enhanced the ALBP porosities and also new porous surfaces were created owing to significant losses of the volatile component(s) and carbon in the form of CO_2 and CO [64]. Therefore, chemical treatment produces ALBP with improved surface areas. It can be seen here that H_3PO_4 assisted in exposing and widening the porosities of locus bean pod residue ACs. The porosity and the large surface

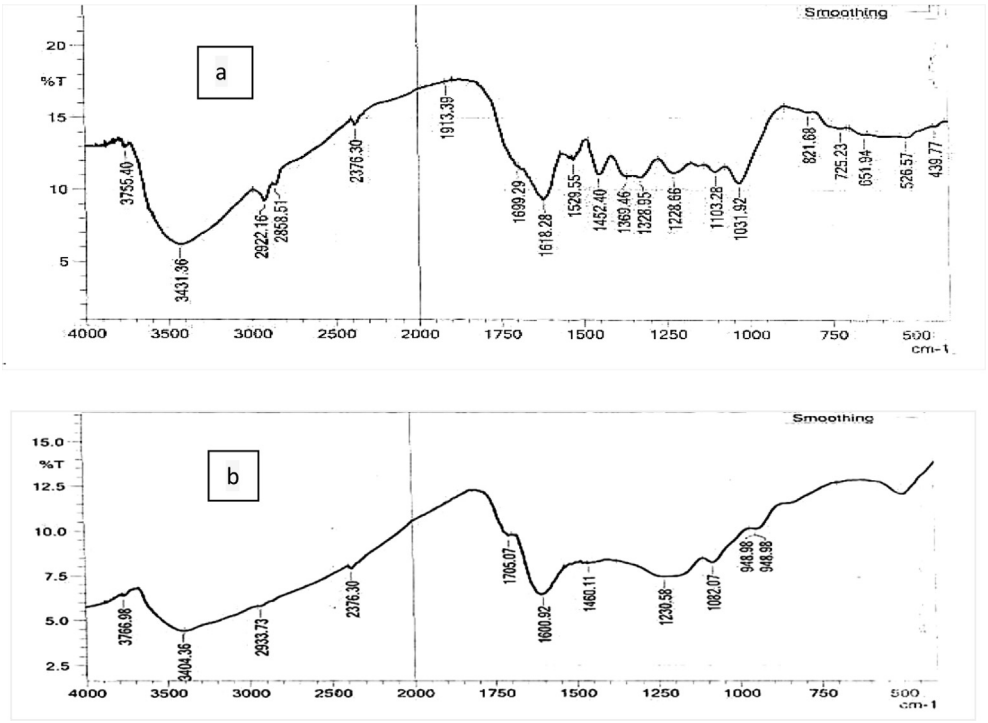

Fig. 1. a. FTIR of Raw locust bean pod (RLBP). b. FTIR of Acid modified locust bean pod (ALBP).

Table 3
Characteristics of raw and acid activated Locust bean pod (LBP) FTIR Spectra.

Wave number (cm^{-1})			Functional groups
RLBP Bands	ALBP Bands	Difference	
3755	3767	+12	Asymmetric stretching of O–H
3431	3404	−27	Bonded O–H group
2922	2934	+12	Aliphatic C–H group
2376	2376	0	-C=N stretching
1699	1705	+6	-C-O stretching of ketone
1618	1601	−17	Aliphatic C=C
1452	1460	−8	C=C stretching in aromatic ring
1369	-	-	C–H bonding in alkane
1229	1231	+2	SO_3 stretching

area structure of ALBP is as a result of highly developed pores, which is a requisite for effective adsorption process [65], these pores in Fig. 2b provides a good surface area of interaction of the adsorbent with Rh–B dye thereby enhancing the adsorption chances of Rh–B dye [6, 49].

3.1.3. Boehm Titration (determination of oxygen containing functional group)

The Boehm technique reveals the surface chemical properties of the adsorbents. Table 4 presents a summary of the properties of the surface functional groups. Prior to the evaluation of surface acidity and basicity; several assumptions were made: (i) acidic groups would only be neutralized by NaOH, Na_2CO_3 or $NaHCO_3$ and (ii) all basic groups are neutralized by HCl. The concentration of the acidic and basic groups are shown in Table 4, The basic group value was lower than the acidic group indicating that the adsorbent surface is predominantly acidic, Similar result was obtained for the adsorption of Barium and Iron ions from aqueous solutions using activated carbon produced from Mazot Ash, [66]. Acidic functional groups results in increased adsorption of Rh–B dye [7, 14].

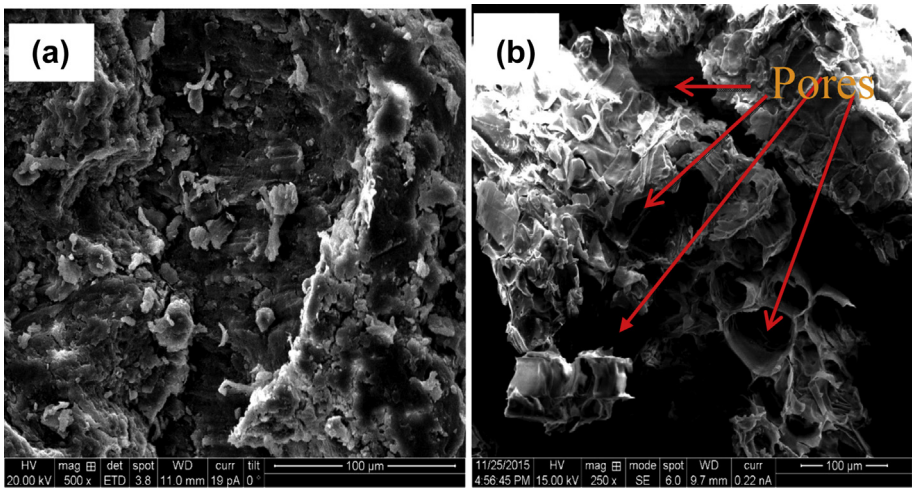

Fig. 2. SEM images of (a) RLBP and (b) ALBP.

Table 4
Different functional groups on ALBP.

Adsorbent	Different functional groups on ALBP				
	Carboxylic mmolg^{-1}	Phenolic mmolg^{-1}	Lactonic mmolg^{-1}	Basic mmolg^{-1}	Acidic mmolg^{-1}
ALBP	1.0862	-	0.2197	0.5172	1.3056

The standard error is ±0.001.

3.1.4. *pH and pH_{PZC} determinations*

The pH point of zero charge (pH_{PZC}) of ALBP was analysed as shown in Fig. 3. The value was determined where the curve cut through the pH_0 axis (Fig. 3). As observed in Fig. 3, the pH_{PZC} was found to be 2.87 for ALBP. The pH value higher than pH_{PZC} enhances adsorption of cation adsorption, while anions adsorption is favoured at a pH value less than pH_{PZC} [7, 41, 65, 67]. Since the pH_{PZC} of ALBP was determined to be at 2.87, it thus suggests that the optimal adsorption is expected to be at pH of 2.87. The effects of pH on the uptake of RhB dye onto ALBP was investigated and the highest percentage of RhB dye adsorbed was obtained at pH 3.1 (95 %) (Fig. 4). A gradual decrease was observed at above pH 3.1. The lowest amount of RhB dye adsorbed was at pH 10.3 (25 %) (Fig. 4). At pH value of 3.0, RhB dye are of cationic and monomeric molecular forms [41], thus the dye molecule can enter easily into the pore structure of ALBP. At pH value higher than pH_{pzc}, the zwitterionic forms of RhB dye exist in solution mixture. This form increases the aggregation of RhB dye molecule to form larger molecules (dimers). The increase in aggregation of the zwitterionic form is due to the attractive electrostatic interactions between the carboxyl and xanthene groups of the monomers [41]. These molecules are unable to enter the pores as a result of their size thereby resulting in lower percentage removal at high pH. Optimum adsorption at pH of 3 has been previously reported in one of our studies on scavenging Rhodamine B dye using *Moringa oleifera* seed pod [41].

3.2. *Batch equilibrium studies*

3.2.1. *Effect of initial dye concentration and contact time*

Fig. 5 shows the effect of initial Rh–B dye concentrations and contact time on the adsorption capacity of ALBP. As the concentration increases with contact time, the q_e value increases. In the first 15mins, the concentration increased steadily, showing a regular or uniform curve at this contact time except 800 and 1000 mg L^{-1} concentrations. The adsorption behavior of Rh–B dye on ALBP adsorbent was investigated in the range of C_0 (200–1000 mg/L) at five levels. The optimum value of C_0 was 1000 mg/L. Increasing the initial dye concentration, adsorption sites will be occupied; thus, occupying the remaining vacant superficial active sites will be difficult due to the interaction (repulsive force) among the dye molecules adsorbed onto the surface [14, 19, 21, 22, 68].The dye uptake increases rapidly as the contact time increases; at a point, the amount of Rh–B dye adsorbed became progressively slow until it attained

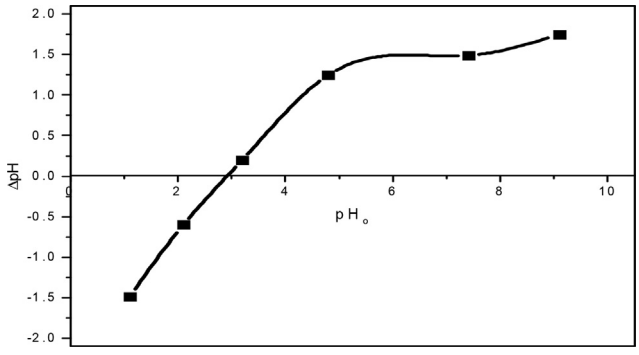

Fig. 3. Plot of pH_{PZC} for ALBP.

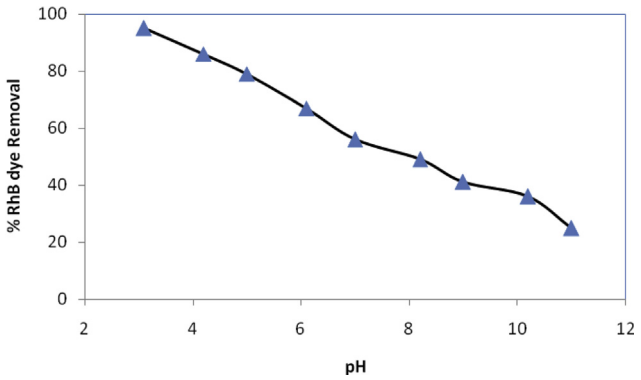

Fig. 4. Percentage Rh–B dye removed using ALBP at different pH.

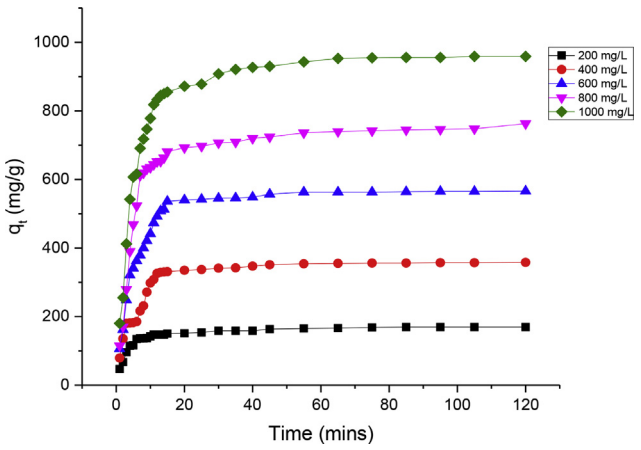

Fig. 5. The effect of contact time and initial Rh–B dye concentration on ALBP at 50 °C.

equilibrium. That is, the amount of dye adsorbed between the intervals of 95–120 min was relatively constant and reached equilibrium. Adsorption studies have shown that the removal of the dye is rapid at initial stage, it however becomes slow on approaching equilibrium [65]. The mass transfer rate between Rh–B dye solution and ALBP was driven by the concentration gradient force [3], hence resulting in higher q_e at higher concentration. Adsorption capacity was enhanced hence, the higher Rh–B dye concentrations provide strong driving forces of the gradients [4]. As the amounts of active ALBP sites became limited, the initial dye concentrations varied; thus, at low dye concentrations, the amounts of ALBP active site has sufficiently accommodated the numbers of Rh–B dye molecules thereby increasing the concentration of the adsorbate as dye molecules became saturated on the active sites. These observations could be in association with great numbers of active vacant sites available on the ALBP surfaces for adsorption in the early stage. Nevertheless, due to the repulsive force that occurs between the adsorbed and free molecule, the remaining vacant surface sites are less available for adsorption as a result of time [65, 69]. Thus, the percentage adsorption processes decrease with increase initial dye concentrations, but the actual amount of dye uptake per unit mass of carbon increases with increased dye concentrations. It can be deduced that the process of adsorption is highly dependent on the initial concentrations of Rh–B dye [37].

3.2.2. *Temperature effects on Rh–B dye adsorption*

The adsorption of Rh–B dye on ALBP was investigated as a function of temperature and maximum dye removal was obtained at 333 K. Experiments were performed at different temperatures (303–333 K) for initial Rh–B dye concentrations of 200–1000 mg/L. It was observed that at temperature below 303 K the amount of dye adsorbed was insignificant;

however, at a temperature above 333 K, the adsorbed amount remains constant. These observations led to the choice of the temperature range used for the study. In this study, it was observed that as solution temperature was increased from 303-333 K, there were significant increase in the adsorption capacities (q_m (mg/g)) from 454.5 to 1111.1 mg/g (Fig. 6), signifying the process of adsorption to be endothermic owing to increase in temperature, thus, the mobility of Rh–B dye molecules increased across ALBP external layers and within its internal pores. At some stages in the adsorption processes, some changes in the structures of the adsorbent and dye took place owing to series of chemical interactions that occurred between the Rh–B dye and ALBP. This further increases the formation of superior affinity existing between ALBP active site and the Rh–B dye. The q_m (mg/g) of the ALBP progresses rapidly with increased in temperatures (i.e. 303K–323K). Temperature increase is also famous for enhancing the diffusion rate [5] and altering or varying the temperature definitely have pronounce effects on equilibrium capacity of Rh–B dye thereby increasing the amount of Rh–B dye molecule to sufficiently acquire energy to undergo interactions with the ALBP active site (s). In addition to this, functionalizing locust bean pod is also expected to contribute significantly to an increased adsorption capacity from 454.5 to 1111.1 mg/g (Fig. 5). This observation is consistent with our earlier study on rambutan seed ACs and other studies [5, 62, 70].

3.3. Adsorption isotherm studies

Fig. 7(a-d) shows the plots of the different isotherms used. Experimental parameters obtained from four different isotherm plots at 50 °C respectively, Langmuir, Freundlich, Temkin, Dubinin-Radushkevich (D-R) are shown in Table 5. Favourability of the process of adsorption was determined by calculating separation factor (R_L) value which was in the range of 0 and 1; this signifies a favourable process of adsorption. Table 4 shows the adsorption energy (E_a) to be 1.12 kJmol^{-1} obtained from D-R isotherm (Fig. 7d) indicating that the removal of Rh–B onto ALBP followed a physisorption process, since the E_a was in the range of 1–8 kJ/mol [49]. The value of R^2 indicates the suitability of isotherm for the Rh–B dye adsorption in the following order: Freundlich ($R^2 = 0.9824$) (Fig. 7b)<D-R ($R^2 = 0.9863$) (Fig. 7d) < Temkin ($R^2 = 0.991$) (Fig. 7c) < Langmuir ($R^2 = 0.9993$) (Fig. 7a) indicating a monolayer adsorption of the Rh–B dye, thereby suggesting that Langmuir model mostly described the process of adsorption. Maximum monolayer adsorption capacity (q_{max}) of 1111.1 mg/g (Table 5) for the Rh–B uptake onto ALBP was obtained. This high adsorption capacity agreed well with our previous study [41]. In comparison with the literature, ALBP exhibits higher adsorption capacity (q_{max}) for Rh–B dye uptake onto ALBP when compared with q_{max} of other adsorbents earlier reported Table 6. The The

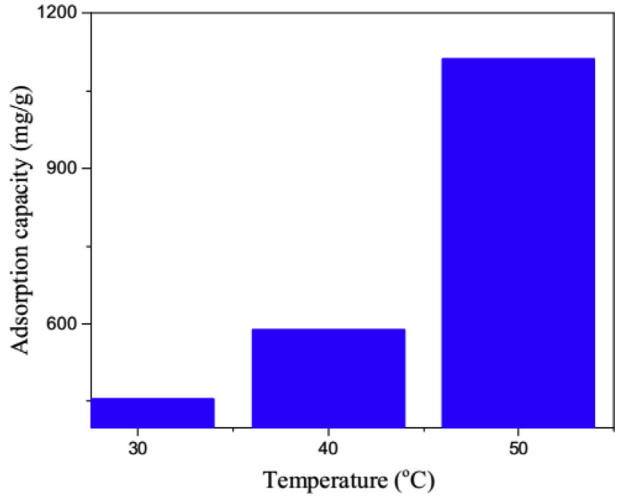

Fig. 6. Effect of solution temperature on RhB dye adsorption unto ALPB.

limits of the many adsorbents compared is low adsorption capacity thus giving the ALBP a superiority over them.

3.4. Adsorption thermodynamic studies

The calculated values of ΔG^0, ΔH^0 and ΔS^0 are important thermodynamic parameters involved in the adsorption process. The values of ΔS° and ΔH° are obtained from the intercept and slope of Van"t Hoff plot of 1/T against In K_L as shown in Fig. 8 which agreed well with our previous studies on malachite green dye adsorption using rambutan seed activated carbon [5]. The positive values of ΔS (280.956 Jmol^{-1}K^{-1}) indicates the affinity of adsorbent for the Rh–B dye uptake and increased randomness at the solid–solution interface during adsorption of Rh–B dye onto the surface of the active sites of ALBP. Table 7 reveals that the negative value of ΔG (-31.892 to -26.355 kJmol^{-1}) depicts the spontaneity and feasibility of the adsorption process, higher negative values were obtained at higher temperature suggesting that at higher temperature, the adsorption process is more spontaneous [38]. Also, the ΔH^0 shows a positive value indicating that the nature adsorption process is endothermic; the calculated thermodynamic parameters are tabulated in Table 7. The adsorption capacity ALBP is dependent on the thermodynamic factors, such as ΔG°, ΔH° and ΔS° [4, 24, 41]. It is also noted that temperature has a considerable effect on the thermodynamic parameters. Similar observation was observed on the temperature effects for the sequestration of cationic dye using sawdust [51, 58].

3.5. Adsorption kinetic and mechanistic studies

The controlling mechanism of the adsorption process was analyzed according to the mathematical expressions given in Eqs. (12), (13), (14), and (15) in Table 2. The optimum operating conditions for designing the purpose and adsorption mechanism is dependent on the kinetics of adsorbate uptake. Four kinetic models namely pseudo-first-order, pseudo-second-order, Elovich and intraparticle diffusion models Fig. 9(a-c) were used in this study to investigate adsorbate uptake onto ALBP, and respective adsorption kinetic parameters obtained for the adsorption of Rh–B dye are shown in Table 8. The kinetic plots are shown in Fig. 9 (a-c). From the data in Table 8, it is clear that the q_e experimental value show some deviation from the q_e calculated, q_e values obtained for pseudo-first-order model from the linear plots in Fig. 9, whereas, for pseudo-second-order model, $q_{e,exp}$ is in good agreement with $q_{e,cal}$ values. Correlation coefficient (R^2) value is usually used to select the best fit. The adsorption kinetics of Rh–B dye fitted best to the pseudo-second order adsorption model with R^2 values higher than pseudo-first order and Elovich models, as shown in Table 8 confirming that the pseudo-second-order rate kinetics described the adsorption data most.

Apart from the three models, the intraparticle diffusion (IPD) parameter was used to determine the mechanism and rate-controlling steps. Fig. 9d shows that the plot is multi-linear, i.e. having three slopes and intercepts, revealing an adsorption mechanism with an increased boundary layer thickness as intercept value increases [4, 41, 65]. The multi-linearity infers that two or more steps took place in the adsorption process inhibiting higher adsorption capacities. Fig. 9d shows the plots of the intraparticle diffusion model. As it was observed in Fig. 9d, the diffusion mechanism at all the concentrations studied (200 mg/L -1000 mg/L) resulted into three multi linear graphs which did not pass through the origin. Since intraparticle diffusion plays a critical role in determining the mechanism of adsorption process, therefore, if the plot of $t^{1/2}$ is a straight line that passes through the origin then it means that the intraparticle diffusion is a rate-limiting step. As seen in Fig. 9d, the deviation from the origin shows that intraparticle diffusion was not the only rate-determining step. Critical observations of Fig. 9d shows that diffusion mechanism was divided into three major phases including (i) rapid diffusion phase which is attributed to the boundary layer diffusion of Rh–B dye molecules unto ALBP owing to the strong electrostatic attraction between the Rh–B solution and the outer surface of the

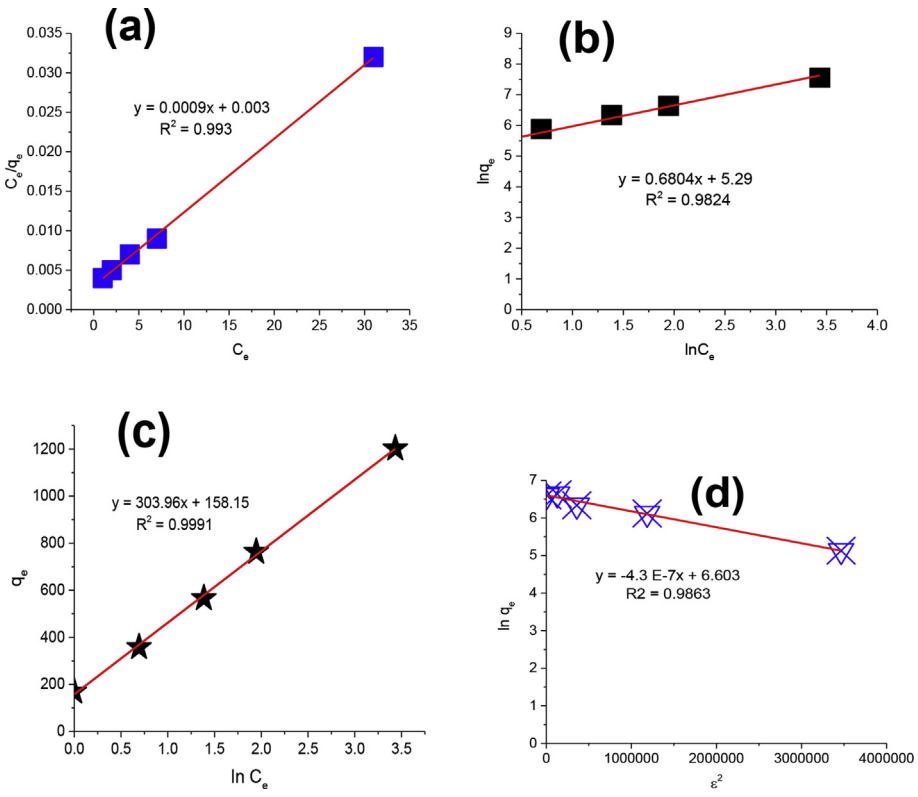

Fig. 7. (a) Langmuir, (b) Freundlich, (c) Tempkin and (d) Dubinin-Radushkevich plots of Rh–B dye adsorption onto ALBP at 50 °C.

Table 5
Isotherm parameters for Rh–B dye adsorption onto ALBP.

Isotherms	Temperature (K)		
	303	313	323
Langmuir			
q_m (mg/g)	454.5	588.2	1111.11
K_L (l/mg)	4.66	4.166	3.333
R_L	0.667	0.29	0.25
R^2	0.999	1	0.9993
Freundlich			
$K_f(mgg^{-1})$ $(mg^{-1})^{1/n}$)	80	139	238
N	2.61	2.95	1.65
1/n	0.383	0.339	0.606
R^2	0.9966	0.9935	0.9996
Tempkin			
K_T (mol/g)	1.1	1.67	1.68
b_T (mol/kJ)	30.1	17.5	8.83
B (L/mg)	83.8	148.8	303.96
R^2=	0.9996	0.9999	0.9991
Dubinin–Radushkevich			
X_m (mg/g)	509.7	712	737.4
B ($mol^2K^1J^2$)	2.0×10^{-5}	1.0×10^{-6}	4.0×10^{-7}
E (KJ/mol)	0.158	0.707	1.12
R^2	0.9361	0.9753	0.9863

The standard error is ±0.001.

adsorbent, (ii) the intraparticle diffusion phase which is a gradual adsorption stage where intraparticle diffusion was the rate determining step, here, the phenomenon of penetration of Rh–B dye molecules into the inner layers of adsorbent occurs gradually. Therefore, the transition that occurred through phases (i) to (ii) reveals the Rh–B dye diffusion from macropores to microporous. (iii) The final equilibrium state where the diffusion became very slow with the reduced Rh–B dye concentrations, stable, approaching plateau profile and equilibrium phase (i. e. maximum). Table 8 shows IPD model parameters, a significant decrease in k_t as time increases for each of the different concentration studied. This

Table 6
Comparison of maximum monolayer adsorption capacities, q_m (mg/g) of Rh–B dye on various adsorbents.

Adsorbents	q_m (mg/g)	References
Irvingia gabonensis	232	[13]
Waste scrap tires	307.2	[42]
Thespusia populinia bark	77.18	[37]
Raphia hookerie fruit epicarp	666.67	[38]
Artocarpusodoratissimus	131	[39]
Perlite	67.935	[40]
Rice husk	518.1	[34]
Casuarina equisetifolia	82.34	[27]
Casuarina equisetifolia	49.5	[36]
Prunus dulcis	32.6	[29]
Locust bean pod	1111.1	*This present study*

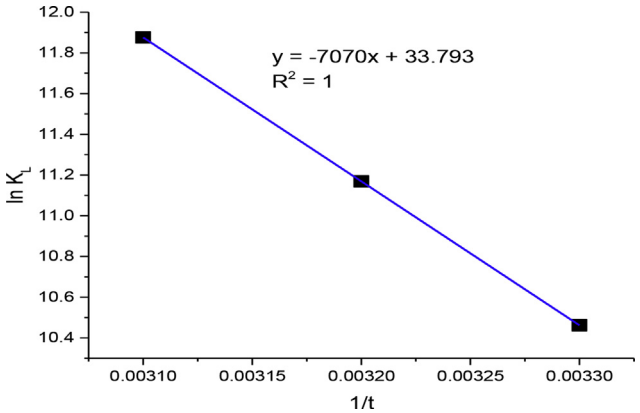

Fig. 8. Van't Hoff plot of 1/T against In K_L for the adsorption of Rh–B dye onto ALBP at different temperatures.

Table 7
Thermodynamic parameters for adsorption of Rh–B dye onto ALBP.

ΔS^o (kJ/mol K)	ΔH^o (kJ/mol)	ΔG^o (kJ/mol)			E_a (kJ mol^{-1})			K_L (l/mg)		
		303 K	303 K	313 K	323K	313 K	323K	323K	313 K	323K
208.956	58.779	−26.355	−26.355	−29.064	0.158	0.707	1.120	4.660	4.166	3.333

The standard error is ±0.001.

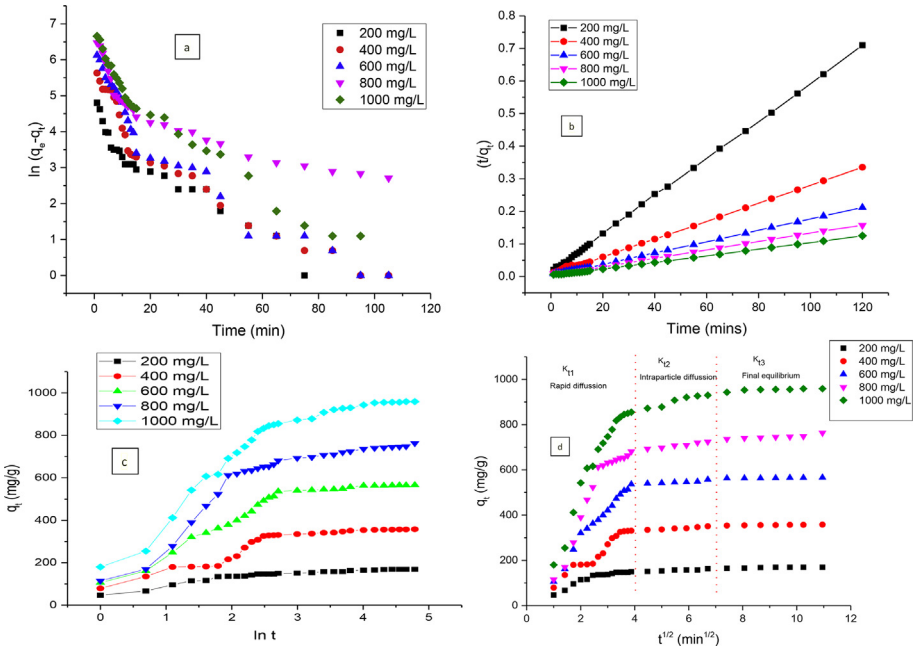

Fig. 9. (a). Plot of Pseudo-first order model for the adsorption of Rh–B dye onto ALBP at 50 °C (b). Plot of Pseudo-second order model for the adsorption of Rh–B dye onto ALBP at 50 °C (c). Plot of Elovich model for the adsorption of Rh–B dye onto ALBP at 50 °C (d). Plot of Intraparticle diffusion model for Rh–B dye adsorption onto ALBP 50 °C.

Table 8
Kinetic parameters for Rh–B dye adsorption onto ALBP at 323K.

Model	Kinetic parameters	Initial Rh–B dye concentration (mg/L)				
		200	400	600	800	1000
Pseudo-second order	k_1 (min^{-1})	0.0263	0.0383	0.0324	0.0361	0.0355
	q_{ecalc} (mg/g)	150	317	372	648	732
	q_{eexp} (mg/g)	169	358	566	763	959
	SSE (%)	4.4	0.2	9.8	9.1	2.9
	H	591.75	3848.73	4483.64	15158.53	19021.75
	R^2	0.9865	0.9689	0.9291	0.9378	0.9919
Pseudo-second order	k_2 (min^{-1})	0.00019	0.00011	0.00012	0.000039	0.00004
	q_{ecalc} (mg/g)	204	385	476	769	909
	q_{eexp} (mg/g)	169	358	566	763	959
	SSE (%)	5.9	12.7	10	31.7	30.6
	H	7.91	16.3	27.19	23.06	33.05
	R^2	0.9941	0.9845	0.9896	0.9511	0.9656
Elovich	β (g/mg)	0.025	0.014	0.011	0.007	0.006
	α [mg/(g min)]	74.9	122.6	114.4	312.6	335.4
	R^2	0.9596	0.9337	0.9529	0.899	0.9097
Intra-particle diffusion	K_{t1} (mg/g h$^{1/2}$)	33.18	90.02	144.35	204.83	240.81
	C_1	1.998	7.918	11.862	25.694	39.009
	R^2	0.8645	0.9560	0.9765	0.8995	0.9475
	K_{t2} (mg/g h$^{1/2}$)	4.82	7.05	6.55	14.43	29.11
	C_2	129.63	302.35	509.33	628.83	741.56
	R^2	0.8897	0.9574	0.8431	0.9707	0.9270
	K_{t3} (mg/g h$^{1/2}$)	1.19	1.06	0.93	6.35	3.83
	C_3	156.94	346.38	555.62	687.36	919.23
	R^2	0.7744	0.9615	0.8989	0.8370	0.7569

The standard error is ±0.001.

Table 9
Price difference between ALBP and CAC.

Cost Description	Price (USD)	
	ALBP (1 Kg)	CAC (1 Kg)
o-phosphoric acid	16.67	-
De-ionized water	10.38	-
Transportation	9.30	4.5
Filter paper	3.60	-
Electricity	2.57	-
Cost of purchase	-	255
Total	42.52	259.5
Difference (CAC- ALBP)	216.98	

implies that external mass transfer is inversely proportional to time. The high values of R^2 revealed the suitability of intraparticle diffusion model in explaining the experimental data. Interestingly as expected, the '*C*" values increase as the initial Rh–B dye concentrations (mg/L) and time increases.

3.6. Cost analysis

The cost analysis presented in Table 9 provides a simple proof that ALBP is approximately six times cheaper than CAC. CAC costs 259.5 USD per kg (transportation inclusive) in total, while ALBP preparation and transportation costs 42.52 USD per kg. The low cost of preparing ALBP as stated in Table 9 gave detailed summary of prices from locus beans pod transportation to filtration and washing of the AC. Ortho-phosphoric acid and deionized water account for most of the significant cost (Table 9).

4. Conclusion

The current study established the promising ability of AC derived from locust bean pod for effective removal of RhB dye from aqueous solution using different concentrations. Analysis by SEM and FTIR spectroscopy's revealed important adsorptive characteristics present in this novel adsorbent. Freundlich, Langmuir, D–R and Temkin isotherms were employed to fit the equilibrium data. Langmuir isotherm best explained the adsorption process having the maximum monolayer coverage (adsorption capacity) of 1111.1 mg/g. The performance of the functionalized-locust bean pod via H_3PO_4-activation was compared with the CAC and previous adsorbents earlier reported. The kinetic of adsorption followed PSO model. The positive values of ΔS (280.956 $Jmol^{-1}K^{-1}$) indicates the affinity of adsorbent for the Rh–B dye uptake and increased randomness at the solid–solution interface during adsorption of Rh–B dye onto the surface of the active sites of ALBP. The negative values of ΔG ranging from -31.892 to -26.355 $kJmol^{-1}$ indicates a spontaneous nature of the process of adsorption, positive ΔH^0 value revealed the endothermic nature of sorption process. The ΔG^0 determined from D–R established a physically controlled process (i.e physisorption). Favourability of the process of adsorption was also established by the separator factor (R_L) value which was in the range of 0 and 1, while the mean adsorption energy (E_a) of 1.12 $kJmol^{-1}$ obtained from D-R isotherm falls within the range of 1–8 kJ/mol, indicating that the removal of Rh–B dye onto ALBP followed a physisorption process. The cost analysis provides a simple proof that ALBP (42.52 USD per kg) is approximately six times cheaper than CAC (259.5 USD per kg). This study therefore; established the feasibility, availability, ease of preparation and eco-friendly nature of locust bean pod as a promising and sustainable adsorbent for effective removal of Rh–B dye from aqueous solutions.

Declarations

Author contribution statement

Olugbenga Solomon Bello: Conceived and designed the experiments; Analyzed and interpreted the data; Contributed reagents, materials, analysis tools or data; Wrote the paper.

Kayode Adesina Adegoke: Analyzed and interpreted the data; Wrote the paper.

Oluwafunmilayo Sarumi, Olasunkanmi Lameed: Performed the experiments; Analyzed and interpreted the data.

Funding statement

This work was supported by The World Academy of Science (TWAS) in form of Research grants; Research Grant number: 11–249 RG/CHE/AF/AC_1_UNESCO FR: 3240262674 (2012), 15–181 RG/CHE/AF/AC_1_: 3240287083 (2015) for the purchase of Research Equipments. NRF-TWAS for Doctoral Fellowship award given to the second author (UID:105453 & Reference: SFH160618172220) and LAUTECH 2016 TET Fund Institution Based Research Intervention (TETFUND/DESS/UNI/OGBOMOSO/RP/VOL. IX) respectively.

Competing interest statement

The authors declare no conflict of interest.

Additional information

No additional information is available for this paper.

References

[1] L. Laasri, M.K. Elamrani, O. Cherkaoui, Removal of two cationic dyes from a textile effluent by filtration-adsorption on wood sawdust, Environ. Sci. Pollut. Control Ser. (2007) 237–240.
[2] K.A. Adegoke, O.S. Bello, Dye sequestration using agricultural wastes as adsorbents, Water Resour Ind 12 (2015) 8–24.
[3] K.A. Adegoke, R.O. Oyewole, B.M. Lasisi, O.S. Bello, Abatement of organic pollutants using fly ash based adsorbents, Water Sci. Technol. 76 (2017) 2580–2592.
[4] T.A. Ojo, A.T. Ojedokun, O.S. Bello, Functionalization of powdered walnut shell with orthophosphoric acid for Congo red dye removal, Part. Sci. Technol. 37 (2019) 74–85.
[5] M.A. Ahmad, N.S. Afandi, K.A. Adegoke, O.S. Bello, Optimization and batch studies on adsorption of malachite green dye using rambutan seed activated carbon, Desalination Water Treat. 57 (2016) 21487–21511.
[6] M.A. Ahmad, N. Ahmad, O.S. Bello, Modified durian seed as adsorbent for the removal of methyl red dye from aqueous solutions, Appl. Water Sci. 5 (2015) 407–423.
[7] M. Farahani, S.R.S. Abdullah, S. Hosseini, S. Shojaeipour, M. Kashisaz, Adsorption-based cationic dyes using the carbon active sugarcane bagasse, Procedia Environ. Sci. (2011).
[8] R.O. Ajemba, A.T. Ojedokun, O.S. Bello, R.O. Ajemba, Adsorption of malachite green from aqueous solution using activated ntezi clay:optimization, isotherm and kinetic studies, Appl. Water Sci. 27 (2014) 839–854.
[9] O.S. Bello, E.S. Owojuyigbe, M.A. Babatunde, F.E. Folaranmi, Sustainable conversion of agro-wastes into useful adsorbents, Appl. Water Sci. 7 (2017) 3561–3571.
[10] Z.A. AlOthman, M.A. Habila, R. Ali, A. Abdel Ghafar, M.S. El-din Hassouna, Valorization of two waste streams into activated carbon and studying its adsorption kinetics, equilibrium isotherms and thermodynamics for methylene blue removal, Arab. J. Chem. (2014).
[11] Z.M. Hussin, N. Talib, N.M. Hussin, M.A.K.M. Hanafiah, W.K.A.W.M. Khalir, Methylene blue adsorption onto NaOH modified durian leaf powder: isotherm and kinetic studies, Am. J. Environ. Eng. 5 (2015) 38–43.
[12] T. Murugan, A. Ganapathi, R. Valliappan, Removal of Dyes from Aqueous Solution by Adsorption on Biomass of Mango (Mangifera Indica) Leaves, 2010.
[13] A.A. INYINBOR, F.A. ADEKOLA, G.A. OLATUNJI, Adsorption of Rhodamine B dye from aqueous solution on Irvingia gabonensis biomass: kinetics and thermodynamics studies, S. Afr. J. Chem. 68 (2015) 115–125.
[14] M.O. Olakunle, A.A. Inyinbor, A.O. Dada, O.S. Bello, Combating dye pollution using cocoa pod husks: a sustainable approach, Int. J. Sustain. Eng. 11 (2018) 4–15.
[15] D.N.E. Thiombiano, N. Lamien, D.S. Dibong, I.J. Boussim, B. Belem, Le rôle des espèces ligneuses dans la gestion de la soudure alimentaire au Burkina Faso, Sci. Changements Planétaires/Sécheresse 23 (2012) 86–93.
[16] S.N. Sylla, R.T. Samba, M. Neyra, I. Ndoye, E. Giraud, A. Willems, P. De Lajudie, B. Dreyfus, Pterocarpus erinaceus, Biosystems 583 (2002) 572–583.
[17] S.K. Fasogbon, A.B. Wahaab, M.O. Oyewola, Thermal comfort characteristics of some selected building materials in the regional setting of Ile-Ife, Nigeria, J. Nat. Resour. Develop. (2016) 54–58.

[18] Z. Teklehaimanot, Exploiting the potential of indigenous agroforestry trees: Parkia biglobosa and Vitellaria paradoxa in sub-Saharan Africa, Agrofor. Syst. (2004) 207–220.
[19] M. Naghizade Asl, N.M. Mahmodi, P. Teymouri, B. Shahmoradi, R. Rezaee, A. Maleki, Adsorption of organic dyes using copper oxide nanoparticles: isotherm and kinetic studies, Desalination Water Treat. 57 (2016) 25278–25287.
[20] N.M. Mahmoodi, U. Sadeghi, A. Maleki, B. Hayati, F. Najafi, Synthesis of cationic polymeric adsorbent and dye removal isotherm, kinetic and thermodynamic, J. Ind. Eng. Chem. 20 (2014) 2745–2753.
[21] K. Salehi, H. Daraei, P. Teymouri, B. Shahmoradi, A. Maleki, Cu-doped ZnO nanoparticle for removal of reactive black 5: application of artificial neural networks and multiple linear regression for modeling and optimization, Desalination Water Treat. 57 (2016) 22074–22080.
[22] B. Hayati, A. Maleki, F. Najafi, F. Gharibi, G. McKay, V.K. Gupta, S. Harikaranahalli Puttaiah, N. Marzban, Heavy metal adsorption using PAMAM/CNT nanocomposite from aqueous solution in batch and continuous fixed bed systems, Chem. Eng. J. (2018).
[23] B. Hayati, N.M. Mahmoodi, A. Maleki, Dendrimer-titania nanocomposite: synthesis and dye-removal capacity, Res. Chem. Intermed. 41 (2015) 3743–3757.
[24] B. Hayati, M. Arami, A. Maleki, E. Pajootan, Thermodynamic properties of dye removal from colored textile wastewater by poly(propylene imine) dendrimer, Desalination Water Treat. 56 (2015) 97–106.
[25] G. Cinelli, F. Cuomo, L. Ambrosone, M. Colella, A. Ceglie, F. Venditti, F. Lopez, Photocatalytic degradation of a model textile dye using Carbon-doped titanium dioxide and visible light, J. Water Process Eng. (2017).
[26] T.S. Anirudhan, M. Ramachandran, Adsorptive removal of basic dyes from aqueous solutions by surfactant modified bentonite clay (organoclay): kinetic and competitive adsorption isotherm, Process Saf. Environ. Prot. 95 (2015) 215–225.
[27] M.R.R. Kooh, M.K. Dahri, L.B.L. Lim, The removal of rhodamine B dye from aqueous solution using Casuarina equisetifolia needles as adsorbent, Cogent Environ. Sci. 2 (2016) 1–14.
[28] J. Fu, Q. Xin, X. Wu, Z. Chen, Y. Yan, S. Liu, M. Wang, Q. Xu, Selective adsorption and separation of organic dyes from aqueous solution on polydopamine microspheres, J. Colloid Interface Sci. (2016).
[29] H.B. Senturk, D. Ozdes, C. Duran, Biosorption of Rhodamine 6G from aqueous solutions onto almond shell (Prunus dulcis) as a low cost biosorbent, Desalination 252 (2010) 81–87.
[30] J. Diamond, 40170, 66 (2001) 40170–40174.
[31] V.J. Cogliano, R. Baan, K. Straif, Y. Grosse, B. Lauby-Secretan, F. El Ghissassi, V. Bouvard, L. Benbrahim-Tallaa, N. Guha, C. Freeman, L. Galichet, C.P. Wild, Preventable exposures associated with human cancers, J. Natl. Cancer Inst. 103 (2010) 1827–1839.
[32] M.S. Field, R.G. Wilhelm, J.F. Quinlan, T.J. Aley, An assessment of the potential adverse properties of fluorescent tracer dyes used for groundwater tracing, Environ. Monit. Assess. 38 (1995) 75–96.
[33] S.D. Sheet, SIGMA-ALDRICH, (2014) 1–8.
[34] L. Ding, B. Zou, W. Gao, Q. Liu, Z. Wang, Y. Guo, X. Wang, Y. Liu, Adsorption of Rhodamine-B from aqueous solution using treated rice husk-based activated carbon, Colloid. Surf. Physicochem. Eng. Asp. 446 (2014) 1–7.
[35] M. Mohammadi, A.J. Hassani, A.R. Mohamed, G.D. Najafpour, Removal of rhodamine b from aqueous solution using palm shell-based activated carbon: adsorption and kinetic studies, J. Chem. Eng. Data 55 (2010) 5777–5785.
[36] M.K. Dahri, M.R.R. Kooh, L.B.L. Lim, Remediation of rhodamine B dye from aqueous solution using Casuarina equisetifolia cone powder as a low-cost adsorbent, Adv.Phys.Chem. 2016 (2016) 1–14.
[37] M. Hema, S. Arivoli, Rhodamine B adsorption by activated carbon: kinetic and equilibrium studies, Indian J. Chem. Technol. (2009).
[38] A.A. Inyinbor, F.A. Adekola, G.A. Olatunji, Kinetics, Isotherms and Thermodynamic Modeling of Liquid Phase Adsorption of Rhodamine B Dye onto Raphia Hookerie Fruit Epicarp, Water Resources and Industry, 2016.
[39] L.B.L. Lim, N. Priyantha, X.Y. Fang, N.A.H. Mohamad Zaidi, Artocarpusodoratissimus peel as a potential adsorbent in environmental remediation to remove toxic Rhodamine B dye, J. Mater. Environ. Sci. (2017).
[40] G. Vijayakumar, R. Tamilarasan, M. Dharmendirakumar, Adsorption, kinetic, equilibrium and thermodynamic studies on the removal of basic dye Rhodamine-B from aqueous solution by the use of natural adsorbent perlite, J. Mater. Environ. Sci. (2012).
[41] O.S. Bello, B.M. Lasisi, O.J. Adigun, V. Ephraim, Scavenging Rhodamine B dye using moringa oleifera seed pod, Chem. Speciat. Bioavailab. 29 (2017) 120–134.
[42] L. Li, S. Liu, T. Zhu, Application of activated carbon derived from scrap tires for adsorption of Rhodamine B, J. Environ. Sci. 22 (2010) 1273–1280.
[43] O.S. Bello, O.C. Alao, T.C. Alagbada, A.M. Olatunde, Biosorption of ibuprofen using functionalized bean husks, Sustain. Chem. Pharm. 13 (2019).
[44] H.P. Boehm, Surface Oxides on Carbon and Their Analysis: A Critical Assessment, Carbon, 2002.
[45] M.J.N.R. Ekpete, O.A. Horsfall, Preparation and characterization of activated carbon derived from fluted pumpkin stem waste (Telfairia occidentalis Hook F), Res. J. Chem. Sci. 1 (2011) 10–17.
[46] I. Langmuir, The adsorption of gases on plane surfaces of glass, mica and platinum, J. Am. Chem. Soc. (1918).
[47] H.M.F. Freundlich, Over the adsorption in solution, J. Phys. Chem. (1906).
[48] V. Temkin, M.J. Pyzhev, Recent modifications to Langmuir isotherms, Acta Physiochim. (1940). URSS.
[49] R.O. Ajemba, Adsorption of malachite green from aqueous solution using activated ntezi clay:optimization, Isotherm Kinetic Stud. 27 (2014) 839–854.
[50] M.M. Dubinin, The potential theory of adsorption of gases and vapors for adsorbents with energetically nonuniform surfaces, Chem. Rev. 60 (1960) 235–241.
[51] S. Lagergren, About the Theory of So-Called Adsorption of Soluble Substances, Handlingar, 1898.
[52] Y.S. Ho, G. McKay, Pseudo-second order model for sorption processes, Process Biochem. 34 (1999) 451–465.
[53] C. Aharoni, M. Ungarish, Kinetics of activated chemisorption. Part 2. - theoretical models, J. Chem. Soc., Faraday Trans. 1: Phys. Chem. Condens.Phases (1977).
[54] M. Ungarish, C. Aharoni, Kinetics of chemisorption. Deducing kinetic laws from experimental data, J. Chem. Soc., Faraday Trans. 1: Phys. Chem. Condens.Phases (1981).
[55] W.J. Weber, J.C. Morris, Kinetics of adsorption on carbon from solution, J. Sanit. Eng. Div. (1963).
[56] O.S. Bello, I.A. Adeogun, J.C. Ajaelu, E.O. Fehintola, Adsorption of methylene blue onto activated carbon derived from periwinkle shells: kinetics and equilibrium studies, Chem. Ecol. 24 (2008) 285–295.
[57] T.W. Weber, R.K. Chakravorti, Pore and solid diffusion models for fixed-bed adsorbers, AIChE J. (1974).
[58] K.R. Hall, L.C. Eagleton, A. Acrivos, T. Vermeulen, Pore- and solid-diffusion kinetics in fixed-bed adsorption under constant-pattern conditions, Ind. Eng. Chem. Fundam. 5 (1966) 212–223.
[59] V. Ponnusami, K.S. Rajan, S.N. Srivastava, Application of film-pore diffusion model for methylene blue adsorption onto plant leaf powders, Chem. Eng. J. 163 (2010) 236–242.
[60] I.A.W. Tan, A.L. Ahmad, B.H. Hameed, Enhancement of basic dye adsorption uptake from aqueous solutions using chemically modified oil palm shell activated carbon, Colloid. Surf. Physicochem. Eng. Asp. 318 (2008) 88–96.
[61] P. Punyapalakul, K. Suksomboon, P. Prarat, S. Khaodhiar, Effects of Surface Functional Groups and Porous Structures on Adsorption and Recovery of Perfluorinated Compounds by Inorganic Porous Silicas, Separation Science and Technology, Philadelphia, 2013.
[62] A. Khasri, O.S. Bello, M.A. Ahmad, Mesoporous activated carbon from Pentace species sawdust via microwave-induced KOH activation: optimization and methylene blue adsorption, Res. Chem. Intermed. 44 (2018) 5737–5757.
[63] O.S. Bello, T.T. Siang, M.A. Ahmad, Adsorption of Remazol Brilliant Violet-5R reactive dye from aqueous solution by cocoa pod husk-based activated carbon: kinetic, equilibrium and thermodynamic studies, Asia Pac. J. Chem. Eng. 7 (2012) 378–388.
[64] M. Auta, B.H. Hameed, Optimized waste tea activated carbon for adsorption of Methylene Blue and Acid Blue 29 dyes using response surface methodology, Chem. Eng. J. 175 (2011) 233–243.
[65] A.T. Ojedokun, O.S. Bello, Kinetic modeling of liquid-phase adsorption of Congo red dye using guava leaf-based activated carbon, Appl. Water Sci. 7 (2017) 1965–1977.
[66] N.M. Hilal, A.A. Emam, N.A. Badawy, A.E. Zidan, Adsorption of barium and Iron ions from aqueous solutions by the activated carbon produced from Mazot ash, Life Sci. J. 10 (2013) 75–83.
[67] A.M.M. Vargas, A.L. Cazetta, M.H. Kunita, T.L. Silva, V.C. Almeida, Adsorption of methylene blue on activated carbon produced from flamboyant pods (Delonix regia): study of adsorption isotherms and kinetic models, Chem. Eng. J. (2011).
[68] A.T. Ojedokun, O.S. Bello, Liquid phase adsorption of Congo red dye on functionalized corn cobs, J. Dispersion Sci. Technol. (2017).
[69] O.S. Bello, M.A. Ahmad, Coconut (cocos nucifera) shell based activated carbon for the removal of malachite green dye from aqueous solutions, Separ. Sci. Technol. 47 (2012) 903–912.
[70] S. Gupta, B.V. Babu, Modeling, simulation, and experimental validation for continuous Cr(VI) removal from aqueous solutions using sawdust as an adsorbent, Bioresour. Technol. 100 (2009) 5633–5640.